





A Port-Hamiltonian Modeling Approach for Integrated Hydrogen Systems

Abdullah Shahin¹ , Hannes Gernandt^{1,2} , Anton Plietzsch¹ , and Johannes Schiffer^{1,3} 

Abstract—Hydrogen’s growing role in the transition towards climate-neutral energy systems necessitates structured modeling frameworks. Existing gas network models, largely developed for natural gas, fail to capture hydrogen systems distinct properties, particularly the coupling of hydrogen pipes with electrolyzers, fuel cells, and electrically driven compressors. In this work, we present a unified systematic port-Hamiltonian (pH) framework for modeling hydrogen systems, which inherently provides a passive input-output map of the overall interconnected system and, thus, a promising foundation for structured analysis, control and optimization of this type of newly emerging energy systems.

I. INTRODUCTION

The shift to climate-neutral energy systems requires integrating various energy carriers, with hydrogen playing a crucial role in decarbonization [1]. Yet, for hydrogen to indeed become a key energy carrier, a dedicated generation and transportation infrastructure along with suitable operation and control structures must be established [2]. Such development is, e.g., already underway in Germany, where a “hydrogen core network” is currently being implemented with planned commissioning in 2032 [3].

For climate-neutrality, the hydrogen production needs to be “green”, i.e., based on renewable energy [4]. Likewise, hydrogen is also foreseen as an important carrier for providing long-term energy storage to electric power systems [2]. This results in a bidirectional energy conversion between electrical and hydrogen domains, so that these systems exhibit complex interdependencies that require structured, modular modeling approaches. Hence, hydrogen network components, which include production, storage, and distribution, must interact seamlessly with electrical grids to facilitate efficient and climate-neutral energy provision.

Clearly, many new control and operational challenges arise for these type of networks. A first step towards addressing these challenges in a structured manner is the development of suitable modeling procedures for systematically assembling

mathematical models of hydrogen systems that reliably capture their fundamental dynamics. This is the main objective pursued in the present paper.

In this context, port-Hamiltonian (pH) systems offer a powerful framework to represent energy-based multi-domain systems, while preserving structural and systemic properties, such as interconnection patterns and passivity [5]. The pH framework has been used successfully to model electric power [6]–[8], heat [9]–[11] and gas networks [12].

In the gas network domain, recently, in [13] a pH representation of lumped gas pipe models and their interconnection has been developed. But therein the focus lies on pipeline dynamics for natural gas systems, omitting hydrogen storage, generation, and load integration, such as electrolyzers and fuel cells. Building on [13], in [14] compressors were introduced into the gas grid model. In [14] the control theoretic properties of a lumped compressor-gas network were analyzed through the establishment of equilibrium-independent passivity (EIP). Additionally, a pH PDE formulation of the gas network including compressors and based on the Euler equations was derived in [15]. Their model explicitly accounts for the enthalpy added to the gas in the compression process, providing a detailed representation of the involved thermodynamics.

Only a few recent studies have considered hydrogen-electric systems within the pH framework. The existing works [16] and [17] primarily focus on the component-level modeling of PEM fuel cells and electrochemical processes, offering insight into the internal dynamics and energy conversion behavior of these individual units. However, these models are not readily extendable to network-scale applications, where the interaction between multiple components and energy carriers must be coherently represented.

In light of this, the main contribution of our work is to adopt a system-level perspective and systematically develop a unified pH model that captures the dynamics of interconnected hydrogen infrastructures. To this end, we first derive individual pH representations for the components of the core hydrogen system, such as pipes, electrolyzers, fuel cells, and electrically driven compressors. Next, by using algebraic graph theory and Kirchhoff’s law to describe the network interconnections, we provide an overall pH model, which ensures structure-preserving interconnections among system components. In this way, the presented approach reveals that hydrogen systems admit a compositional pH structure, which inherently provides a passive input-output map of the overall interconnected system and, thus, a promising foundation for structured analysis, control, and optimization of this type of

This work was supported by the European Union’s Horizon Europe Framework Programme (HORIZON) under the GA n. 101120278 - DENSE. HG and JS acknowledge funding from the German Federal Government, the Federal Ministry of Education and Research, and the State of Brandenburg within the framework of the joint project EIZ: Energy Innovation Center (project numbers 85056897 and 03SF0693A)

¹Fraunhofer IEG, Fraunhofer Research Institution for Energy Infrastructures and Geotechnologies IEG, 03046 Cottbus, Germany, {abdullah.shahin, anton.plietzsch}@ieg.fraunhofer.de,

²Institute of Mathematical Modelling, Analysis and Computational Mathematics IMACM, University of Wuppertal, 42119 Wuppertal, Germany, gernandt@uni-wuppertal.de

³Brandenburg University of Technology Cottbus-Senftenberg, 03046 Cottbus, Germany, schiffer@b-tu.de

newly emerging energy systems.

The remainder of this paper is structured as follows: In Section II, we recall the class of pH systems. The pH models of the hydrogen grid components are presented in Section III. In Section IV the interconnection and integration of hydrogen components in an interconnected system is described.

Notation. We employ the following short-hands. For $\ell > 1$ scalars $v_i, i = 1, \dots, \ell$, $v = (v_i)_{i=1}^\ell \in \mathbb{R}^\ell$ denotes a column vector, whose entries are v_i . For $v \in \mathbb{R}^\ell$ and $w \in \mathbb{R}^{\ell'}$, where $\ell' > 1$, we denote $(v, w) \in \mathbb{R}^{\ell+\ell'}$ as a column vector containing the entries of v and w . Given $\ell > 1$ matrices $M_i \in \mathbb{R}^{n_i \times m_i}, i = 1, \dots, \ell$, the notation $\text{diag}(M_i)_{i=1}^\ell \in \mathbb{R}^{(\sum_{i=1}^\ell n_i) \times (\sum_{i=1}^\ell m_i)}$ denotes the block matrix, whose block elements are M_i . The identity matrix of size $k \times k$ is denoted by I_k . Furthermore, the zero matrix of size $k \times l$ is denoted by $0_{k \times l}$ and in the case $l = 1$ we simply write $0_k \in \mathbb{R}^k$.

II. PORT-HAMILTONIAN SYSTEMS

In the following, we recall from [18] the form of pH systems employed throughout the paper

$$\begin{aligned} \dot{x} &= (J(x) - R(x))\nabla H(x) + Bu + d, \\ y &= B^\top \nabla H(x) + Du, \end{aligned} \quad (1)$$

where $H : \mathbb{R}^n \rightarrow [0, \infty)$ is the Hamiltonian, which is assumed to be continuously differentiable with gradient $\nabla H(x)$, $B \in \mathbb{R}^{n \times m}$ is the input matrix, $D \in \mathbb{R}^{m \times m}$ is the feedthrough matrix and $d \in \mathbb{R}^n$ is a constant disturbance. Furthermore, the interconnection and damping matrices $J : \mathbb{R}^n \rightarrow \mathbb{R}^{n \times n}$ and $R : \mathbb{R}^n \rightarrow \mathbb{R}^{n \times n}$, respectively, satisfy the following structural conditions for all $x \in \mathbb{R}^n$,

$$J(x) = -J(x)^\top \quad R(x) = R(x)^\top \geq 0, \quad D + D^\top \geq 0.$$

This directly implies that in the unperturbed case, i.e. $d \equiv 0$, the system (1) is passive [18], i.e. the time derivative of the Hamiltonian H along the solutions of the system (1) satisfies

$$\begin{aligned} \dot{H} &= -\nabla H^\top R(x) \nabla H + \nabla H^\top Bu \\ &= -\nabla H^\top R(x) \nabla H + y^\top u - \frac{1}{2} u^\top (D + D^\top) u \leq y^\top u. \end{aligned}$$

III. PORT-HAMILTONIAN MODELING OF HYDROGEN SYSTEMS

In this section, we introduce pH models for pipes, compressors and storage units and also develop pH representations for electrolyzers and fuel cells.

A. Network topology

The hydrogen network topology is described by an undirected, connected graph $\mathcal{G} = (\mathcal{N}, \mathcal{E})$ with set of nodes $\mathcal{N} = \{n_1, \dots, n_N\}$ and set of edges $\mathcal{E} = \{e_1, \dots, e_M\}$. To each node $n_i \in \mathcal{N}$, we associate a node pressure $\mathbf{p}_i \in \mathbb{R}$. Moreover, to each edge $e_\ell = \{n_i, n_k\} \in \mathcal{E}$, we associate a volumetric flow rate $\mathbf{q}_\ell \in \mathbb{R}$ and assign an arbitrary direction to each edge. Then, if \mathbf{q}_ℓ is directed from n_i to n_k , we call n_i the source of e_ℓ and n_k the sink of e_ℓ and we write $e_\ell = \overrightarrow{n_i n_k}$. It is convenient to introduce the node-edge incidence matrix

$B_G = (b_{ij}) \in \mathbb{R}^{N \times M}$, which is defined by

$$b_{ij} = \begin{cases} 1 & \text{if node } n_i \text{ is the sink of edge } e_j, \\ -1 & \text{if node } n_i \text{ is the source of edge } e_j, \\ 0 & \text{otherwise.} \end{cases} \quad (2)$$

We consider a hydrogen system that contains $S \geq 1$ storage units, $F \geq 1$ junctions, and $C \geq 1$ compressors. The set of nodes \mathcal{N} is thus subdivided into the set $\mathcal{N}_S = \{n_1, \dots, n_S\}$ that represents storage units, the set $\mathcal{N}_F = \{n_{S+1}, \dots, n_{S+F}\}$ that represents junctions within the hydrogen grid and the set of compressors $\mathcal{N}_C = \{n_{S+F+1}, \dots, n_{S+F+C}\}$, with $n_{S+F+C} = n_N$ and $\mathcal{N} = \mathcal{N}_S \cup \mathcal{N}_F \cup \mathcal{N}_C$.

The hydrogen system is coupled to the electric domain via $E \geq 0$ electrolyzers and $L \geq 0$ fuel cells. The interconnection topology between the electric power system and the hydrogen system is modeled by a second undirected graph $\mathcal{G}_P = (\mathcal{N}_S \cup \mathcal{N}_P, \mathcal{E}_P)$. As commonly done in practice, we assume that each power conversion device is always connected to a dedicated storage unit on the hydrogen side, i.e., to a node $n_i \in \mathcal{N}_S$. Hence, $E + L \leq S$. Consequently, the corresponding buses in the electrical power system are represented by the set $\mathcal{N}_P = \{n_{P,1}, \dots, n_{P,E+L}\}$. To each $n_{P,i} \in \mathcal{N}_P$, we associate a voltage $\mathbf{v}_i \in \mathbb{R}$. Furthermore, each pair of nodes $\{n_i, n_{P,i}\}$ is interconnected by an edge $e_{P,k} = \{n_i, n_{P,i}\} \in \mathcal{E}_P$ with $\mathcal{E}_P = \{e_{P,1}, \dots, e_{P,E+L}\}$, where the edge $e_{P,k} \in \mathcal{E}_P$ represents the volumetric flow rate between a fuel cell or an electrolyzer and the hydrogen grid, respectively.

In the sequel, we focus on developing the main components of a sector coupled hydrogen system. The vector of pressures of the hydrogen system is denoted by $\mathbf{p} = (\mathbf{p}_i)_{i=1}^N$ and that of the volumetric flow rates by $\mathbf{q} = (\mathbf{q}_i)_{i=1}^M$. Moreover, we introduce the vector of exogenous volumetric flow rates $\mathbf{q}_{\text{ex}} = (\mathbf{q}_{\text{ex},i})_{i=1}^{S+F} \in \mathbb{R}^{S+F}$, that is used to represent exogenous hydrogen injections or demands stemming, e.g., from onshore terminals.

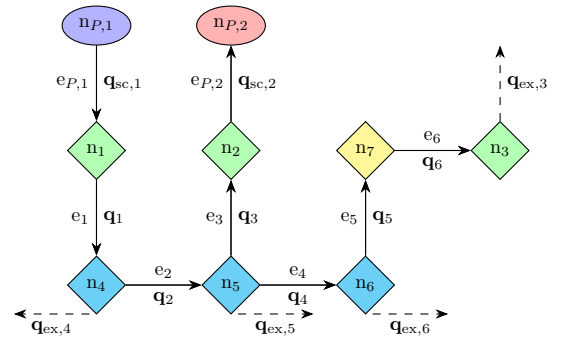


Fig. 1. Example hydrogen network topology. The symbols denote the following elements: \diamond storage unit \mathcal{N}_S , \diamond junction \mathcal{N}_F , \diamond compressor \mathcal{N}_C , \circ electrolyzer \mathcal{N}_P , \circ fuel cell \mathcal{N}_P . Arrows indicate the volumetric flow rates in pipelines $\mathbf{q}_1, \mathbf{q}_2, \mathbf{q}_3, \mathbf{q}_4$, compressors \mathbf{q}_5 and \mathbf{q}_6 , electrolyzer outlet $\mathbf{q}_{\text{sc},1}$, fuel cells inlet $\mathbf{q}_{\text{sc},2}$ and exogenous volumetric flow rates $\mathbf{q}_{\text{ex},i}$.

B. Pipe model

The hydrogen pipe associated with the i th edge $e_i = \{n_l, n_r\} \in \mathcal{E}$, $n_l \in \mathcal{N}_S \cup \mathcal{N}_F$, $n_r \in \mathcal{N}_S \cup \mathcal{N}_F$, is considered to be a spatially one-dimensional object and the temporal change of pressure and volumetric flow rate of the hydrogen along the pipe can be described in terms of the isothermal compressible Euler equation, see e.g. [12]. A simplified lumped model which models the volumetric flow rate \mathbf{q}_i at standard conditions and with a constant compressibility factor was described in [13, Proposition 2] and is given by

$$\rho \frac{\dot{\mathbf{q}}_i}{A_i} = \frac{\mathbf{p}_l - \mathbf{p}_r}{L_i} - \hat{\lambda}_i |\mathbf{q}_i| \mathbf{q}_i - \frac{g \sin(\theta_i)}{c^2} \mathbf{p}_{M,i}, \quad (3)$$

with pressures \mathbf{p}_l and \mathbf{p}_r at the left and right ends of the pipeline segment, respectively, the cross-sectional area $A_i > 0$, the diameter $D_i > 0$, the pipe-length $L_i > 0$, the speed of sound in hydrogen $c > 0$, hydrogen density at standard conditions $\rho > 0$, a friction coefficient

$$\hat{\lambda}_i = \frac{\lambda c^2 \rho^2}{2 D_i A_i^2 \mathbf{p}_{M,i}},$$

with Darcy friction factor $\lambda > 0$, pipe inclination angle $\theta_i \in [-\pi/2, \pi/2]$ and the gravitational acceleration $g > 0$.

Moreover, $\mathbf{p}_{M,i} > 0$ is the mean pressure across the i th pipeline segment given by the Weymouth mean pressure

$$\mathbf{p}_{M,i} = \frac{2}{3} \frac{\mathbf{p}_l^3 - \mathbf{p}_r^3}{\mathbf{p}_l^2 - \mathbf{p}_r^2} = \frac{2}{3} \left(\mathbf{p}_l + \mathbf{p}_r - \frac{\mathbf{p}_l \mathbf{p}_r}{\mathbf{p}_l + \mathbf{p}_r} \right). \quad (4)$$

To model the hydrogen flow rate within a pipe, we consider the following standard modeling assumptions, see also [13].

Assumption 1: In the model (3), the inclination angle θ_i and the mean pressure $\mathbf{p}_{M,i}$ given by (4) are constant.

With Assumption 1 and by introducing the states, Hamiltonian and co-states

$x_{e,i} = \rho \frac{L_i}{A_i} \mathbf{q}_i$, $H_{e,i}(x_{e,i}) = \frac{A_i}{2L_i\rho} \|x_{e,i}\|^2$, $\nabla H_{e,i}(x_{e,i}) = \mathbf{q}_i$, the pipe model (3) can be cast in the following pH form, see also [13, Theorem 3],

$$\begin{aligned} \dot{x}_{e,i} &= (J_{e,i} - R_{e,i}(x_{e,i})) \nabla H_{e,i}(x_{e,i}) + B_{e,i} u_{e,i} + d_{e,i}, \\ y_{e,i} &= B_{e,i}^\top \nabla H_{e,i}(x_{e,i}) = \mathbf{q}_i, \quad u_{e,i} = \mathbf{p}_l - \mathbf{p}_r, \\ d_{e,i} &= -\frac{g L_i \sin(\theta_i)}{c^2} \mathbf{p}_{M,i}, \end{aligned} \quad (5)$$

$$B_{e,i} = 1 \quad J_{e,i} = 0, \quad R_{e,i}(x_{e,i}) = \hat{\lambda}_i L_i \frac{A_i}{L_i \rho} |x_{e,i}|.$$

As shown in [13], the lumped model (5) achieves an accuracy comparable to advanced discretized pipeline models [19]. Also, with Assumption 1, $R_{e,i}(x_{e,i}) \geq 0$ holds for all $x_{e,i} \in \mathbb{R}$. In comparison with [13], we do not incorporate the pressure dynamics of the boundary nodes of the pipe directly into the model (3). Instead, we incorporate these pressure dynamics in the junction and storage unit models, since this simplifies the modular interconnection of the individual network components.

C. Hydrogen storage unit model

In this section, we describe a general model of a hydrogen storage unit connected at node $n_i \in \mathcal{N}_S$ with pressure \mathbf{p}_i and

which is interconnected via two edges $e_l \in \mathcal{E}$ and $e_k \in \mathcal{E}$. Then, the dynamics is given by [20]

$$\frac{M_{H_2} V_{s,i}}{\rho R T_{s,i}} \dot{\mathbf{p}}_i = -\rho^{-1} r_{s,i} \mathbf{p}_i + \mathbf{q}_{in,i} - \mathbf{q}_{out,i} + \mathbf{q}_{ex,i}, \quad (6)$$

where $V_{s,i} > 0$ is the storage unit volume, $M_{H_2} > 0$ is the molar mass of the stored hydrogen, $\mathbf{q}_{in,i}$ is the ingoing volumetric flow rate from the grid to the node n_i , $\mathbf{q}_{out,i}$ is the outgoing volumetric flow rate from the node n_i into the grid, $\mathbf{q}_{ex,i}$ is a volumetric flow rate that represents exogenous hydrogen injections or demands, $T_{s,i} > 0$ is the temperature of the stored hydrogen, which is assumed to be constant, and $R = 8.314 \text{ J}/(\text{mol} \cdot \text{K})$ is the universal gas constant. Moreover, to account for potential storage unit losses, such as leakage, we introduce a dissipation constant $r_{s,i} > 0$.

To write the dynamics (6) in pH form, we introduce

$$x_{n,i} = \frac{M_{H_2} V_{s,i}}{\rho R T_{s,i}} \mathbf{p}_i, \quad H_{n,i}(x_{n,i}) = \frac{1}{2} \frac{\rho R T_{s,i}}{M_{H_2} V_{s,i}} x_{n,i}^2,$$

$$R_{n,i} = r_{s,i} \geq 0, \quad J_{n,i} = 0, \quad B_{n,i} = \begin{bmatrix} 1 & 1 \end{bmatrix},$$

and define the output as well as the input

$$y_{n,i} = B_{n,i}^\top \nabla H_{n,i}(x_{n,i}) = \begin{bmatrix} \mathbf{p}_i \\ \mathbf{p}_i \end{bmatrix}, \quad u_{n,i} = \begin{bmatrix} \mathbf{q}_{in,i} - \mathbf{q}_{out,i} \\ \mathbf{q}_{ex,i} \end{bmatrix}.$$

With this, we obtain from (6) the following pH model

$$\begin{aligned} \dot{x}_{n,i} &= -R_{n,i} \nabla H_{n,i}(x_{n,i}) + B_{n,i} u_{n,i}, \\ y_{n,i} &= B_{n,i}^\top \nabla H_{n,i}(x_{n,i}). \end{aligned} \quad (7)$$

D. Junction model

Based on the considerations in [13] we describe a junction between different pipes at a node $n_i \in \mathcal{N}_F$ by the following equation for the node pressure

$$C_i \dot{\mathbf{p}}_i = \mathbf{q}_{in,i} - \mathbf{q}_{out,i} + \mathbf{q}_{ex,i}, \quad C_i = \sum_{l=1, n_l \in e_l}^M \frac{L_l A_l}{2 \rho c^2},$$

where $C_i > 0$ models a lumped storage capacity at the junction node n_i and we sum in the definition of C_i over all edges that are incident with the node n_i . Our junction model can be viewed as a lossless storage with a comparably small storage capacity C_i and accordingly, the pH formulation of junctions is given similar to (7) with

$$\begin{aligned} x_{n,i} &= C_i \mathbf{p}_i, \quad H_{n,i}(x_{n,i}) = \frac{1}{2} C_i^{-1} x_{n,i}^2, \\ R_{n,i} &= 0, \quad J_{n,i} = 0, \quad B_{n,i} = \begin{bmatrix} 1 & 1 \end{bmatrix}. \end{aligned} \quad (8)$$

E. Compressor unit model

We consider a centrifugal compressor at node $n_i \in \mathcal{N}_C$, which is modeled according to [21]. That is, we describe the pressure dynamics within the plenum \mathbf{p}_i and using the input pressure \mathbf{p}_l at the inlet grid node $n_l \in \mathcal{N}_S \cup \mathcal{N}_F$ and the pressure \mathbf{p}_r at the outlet node $n_r \in \mathcal{N}_S \cup \mathcal{N}_F$ that receives the volumetric flow rate from the plenum \mathbf{p}_i . This means that the corresponding volumetric flow rates \mathbf{q}_f towards the plenum and from the plenum to the grid, \mathbf{q}_m , are represented via the volumetric flow rates over the edges $e_f = \{n_l, n_i\} \in \mathcal{E}$ and

$e_m = \{n_i, n_r\} \in \mathcal{E}$. Thus, the dynamics are

$$\begin{aligned} \frac{V_{p,i}}{\rho a_{01,i}^2} \dot{\mathbf{p}}_i &= -\rho^{-1} r_{pl,i} \mathbf{p}_i + \mathbf{q}_f - \mathbf{q}_m, \\ \frac{\rho L_{c,f}}{A_{1,f}} \dot{\mathbf{q}}_f &= \mathbf{p}_{2,f} - \mathbf{p}_i, \\ \frac{\rho L_{o,m}}{A_{o,m}} \dot{\mathbf{q}}_m &= \mathbf{p}_i - \mathbf{p}_r, \end{aligned} \quad (9)$$

where $a_{01,i} > 0$ is the inlet stagnation sonic velocity, $V_{p,i} > 0$ is the volume of the plenum, $L_{c,f} > 0$ is the length of compressor and duct, $L_{o,m} > 0$ the length of the compressor outlet, $A_{1,f} > 0$, $A_{o,m} > 0$ are the reference areas, $\mathbf{p}_{2,f}$ is the output pressure of the compressor and $r_{pl,i} > 0$ is a coefficient accounting for pressure losses in the plenum.

Adherent to the methodology proposed in [15], the differential pressure across the compressor $\Delta \mathbf{p}_j$ is used as a control input, i.e.,

$$\mathbf{p}_{2,f} = \mathbf{p}_{2,f} - \mathbf{p}_l + \mathbf{p}_l, \quad \Delta \mathbf{p}_{i-N+C} := \mathbf{p}_{2,f} - \mathbf{p}_l, \quad (10)$$

where the node index i fulfills $i \in \{N - C + 1, \dots, N\}$ and therefore $i - N + C \in \{1, \dots, C\}$.

In the following, we split the compressor model into three pH submodels: the pressure node dynamics in the plenum which can be modeled as a storage node (7) with

$$\begin{aligned} x_{n,i} &= \frac{V_{p,i}}{\rho a_{01,i}^2} \mathbf{p}_i, \quad H_{n,i}(x_{n,i}) = \frac{1}{2} \frac{\rho a_{01,i}^2}{V_{p,i}} x_{n,i}^2, \quad d_{n,i} = 0, \\ R_{n,i} &= \frac{r_{pl,i}}{\rho}, \quad J_{n,i} = 0, \quad B_{n,i} = 1, \quad u_{n,i} = \mathbf{q}_f - \mathbf{q}_m. \end{aligned} \quad (11)$$

Secondly, the volumetric flow rate through the throttle can be modeled analogously to the pH pipe model (5) with

$$\begin{aligned} x_{e,m} &= \frac{\rho L_{o,m}}{A_{o,m}} \mathbf{q}_m, \quad H_{e,m}(x_{e,m}) = \frac{1}{2} \frac{A_{o,m}}{\rho L_{o,m}} x_{e,m}^2, \quad d_{e,m} = 0, \\ R_{e,m} &= J_{e,m} = 0, \quad B_{e,m} = 1, \quad u_{e,m} = \mathbf{p}_i - \mathbf{p}_r. \end{aligned} \quad (12)$$

Similarly, the volumetric flow rate dynamics through the compressor towards the plenum can be modeled analogously to the pH pipe model (5) with

$$x_{e,f} = \frac{\rho L_{c,f}}{A_{1,f}} \mathbf{q}_f, \quad H_{e,f}(x_{e,f}) = \frac{A_{1,f}}{2 \rho L_{c,f}} x_{e,f}^2, \quad d_{e,f} = 0, \quad (13)$$

$$R_{e,f} = J_{e,f} = 0, \quad B_{e,f} = \begin{bmatrix} 1 & 1 \end{bmatrix}, \quad u_{e,f} = \begin{bmatrix} \mathbf{p}_l - \mathbf{p}_i \\ \Delta \mathbf{p}_f \end{bmatrix}.$$

Remark 1: Following [21] one can also impose closed coupled valve control to replace the pressure difference $\Delta \mathbf{p}_f$ in (10) by a desired dissipating term. Additionally, the model could be augmented by incorporating the compressor shaft's rotational speed ω as a state variable, with compressor torque as the control input.

F. Sector coupling components

In this section, we present lumped pH electrolyzer and fuel cell models that facilitate the integration of the hydrogen system with the electrical domain that can be used for control from a macroscopic grid perspective of an integrated hydrogen network. Recall from Section III-A that the interconnection topology between the hydrogen system

and the electric power system is modeled by the graph $\mathcal{G}_P = (\mathcal{N}_F \cup \mathcal{N}_P, \mathcal{E}_P)$.

First, we describe the electrolyzer model. Due to the increased integration and the increase in the dimensioning of the electrolyzers, it becomes crucial to model the electric dynamic behavior of the electrolyzer [22]. We focus on polymer exchange membrane (PEM) electrolyzers and follow the modeling in [23] to obtain a model that provides a dynamic description of the voltage and current dynamics as well as the outgoing hydrogen volumetric flow rates.

The electrical dynamics of the electrolyzer represented by the node $n_{P,i} \in \mathcal{N}_P$ is essentially described by the activation overpotential $\mathbf{v}_{a,i}$, which is a key component of the electrolyzer voltage that is mainly influenced by the reaction kinetics of the electrochemical process. It reflects the additional energy required to overcome the activation energy barrier for the hydrogen and oxygen evolution reactions.

The activation overpotential $\mathbf{v}_{a,i}$ can be modeled by [23]

$$C_{a,i} \dot{\mathbf{v}}_{a,i} = \mathbf{i}_i - R_{a,i}^{-1} \mathbf{v}_{a,i}, \quad (14)$$

where $\mathbf{i}_i \in \mathbb{R}$ is the total electrolyzer current, $R_{a,i} > 0$ is the activation resistance, $C_{a,i} = \frac{C_{DL,cell,i} A_i}{n_{c,i}} > 0$ is the total double-layer capacitance, based on the cell surface area A_i and $C_{DL,cell,i}$ is the cell capacitance and $n_{c,i}$ is the number of cells.

The total electrolyzer voltage \mathbf{v}_i at the electrical node $n_{P,i} \in \mathcal{N}_P$ is given as [23]

$$\mathbf{v}_i = \mathbf{v}_{oc,i} + \mathbf{v}_{a,i} + \mathbf{v}_{oh,i}, \quad (15)$$

with $\mathbf{v}_{oc,i}$ being the open-circuit voltage of the electrolyzer, as described by the Nernst equation, i.e.,

$$\mathbf{v}_{oc,i} = n_{c,i} \left(\mathbf{v}_{st} - \beta_T (T_i - T_{st}) + \frac{RT_i}{2F} \ln \left(\frac{p_{H_2}}{\sqrt{p_{O_2} p_{H_2O}}} \right) \right),$$

where $\beta_T = 0.0009 \text{ V/K}$ is the temperature coefficient accounting for the variation of the open-circuit voltage with temperature $T_i > 0$ and $F \approx 9.6485 \cdot 10^4 \text{ C/mol}$ is the Faraday constant. The cell voltage under standard conditions \mathbf{v}_{st} is typically 1.23 V. Standard conditions are defined as a temperature of $T_{st} = 298.15 \text{ K}$ and a pressure of $P_{st} = 101325 \text{ Pa}$, and $p_{H_2}, p_{O_2}, p_{H_2O}$ are the partial pressures of hydrogen, oxygen, and water [24].

The Ohmic overpotential $\mathbf{v}_{oh,i}$ accounts for resistive losses in the electrolyte and electrodes and is given by

$$\mathbf{v}_{oh,i} = n_{c,i} \frac{\delta_{m,i}}{\sigma_{m,i} A_i} \mathbf{i}_i, \quad (16)$$

with membrane thickness and conductivity $\delta_{m,i}, \sigma_{m,i} > 0$.

The fuel cell can be thought of as the counterpart to an electrolyzer, i.e. hydrogen is consumed to produce electrical power.

Thus, the dynamics of the activation overpotential $\mathbf{v}_{a,i}$ at the fuel cell node $n_{P,i} \in \mathcal{N}_P$ in terms of the fuel cell current \mathbf{i}_i is identical to the electrolyzer behavior (14) and the total fuel cell voltage \mathbf{v}_i is given by [25]

$$-\mathbf{v}_i = -\mathbf{v}_{oc,i} + \mathbf{v}_{a,i} + \mathbf{v}_{oh,i}, \quad (17)$$

with its output power depending on the hydrogen input flow rate. The volumetric flow rate of hydrogen can be expressed

in terms of the electrolyzer and fuel cell currents \mathbf{i}_i as [26]

$$\mathbf{q}_{\text{sc},i} = \frac{M_{\text{H}_2}}{z\rho F} \mathbf{i}_i, \quad (18)$$

where $M_{\text{H}_2} = 2.016 \text{ g/mol}$ is the molar mass of hydrogen, $z = 2$ is the number of electrons transferred per hydrogen molecule.

Assumption 2: Consider the electrolyzer and fuel cell dynamics (14), (15), and (17). (i) The open circuit voltage $\mathbf{v}_{\text{oc},i}$ is constant for all $i = 1, \dots, E + L$;

(ii) The activation resistance $R_{a,i}$ is constant for all $i = 1, \dots, E + L$.

Assumption 2 is valid for moderate temperature changes within the electrolyzer and the fuel cell stacks, i.e., if the electrolyzers and fuel cells are operated relatively close to some desired operating state for the hydrogen volumetric flow rates and the temperature dynamics. This is reasonable in many settings, since often additional temperature control is applied to achieve a specific temperature set-point [23], [27]. For larger temperature changes, the irreversible pH framework [28] could be employed to derive a model that captures the associated thermodynamic more accurately.

Furthermore, a suitable constant value for the activation resistance $R_{a,i}$ can be identified in experimental setups from measurement data [29].

With Assumption 2, we can rewrite the electrolyzer dynamics (14) and (15) and the fuel cell dynamics (17), (18) as the following pH system with feed-through

$$\begin{aligned} \dot{x}_{\text{sc},i} &= (J_{\text{sc},i} - R_{\text{sc},i}) \nabla H_{\text{sc},i}(x_{\text{sc},i}) + B_{\text{sc},i} u_{\text{sc},i}, \\ y_{\text{sc},i} &= B_{\text{sc},i}^\top \nabla H_{\text{sc},i}(x_{\text{sc},i}) + D_{\text{sc},i} u_{\text{sc},i} + d_{\text{sc},i}, \\ H_{\text{sc},i}(x_{\text{sc},i}) &= \frac{1}{2} C_{a,i}^{-1} x_{\text{sc},i}^2, \quad x_{\text{sc},i} = C_{a,i} \mathbf{v}_{a,i}, \\ u_{\text{sc},i} &= \mathbf{q}_{\text{sc},i}, \quad d_{\text{sc},i} = \begin{cases} \frac{z\rho F}{M_{\text{H}_2}} \mathbf{v}_{\text{oc},i} & \text{if } 1 \leq i \leq E, \\ -\frac{z\rho F}{M_{\text{H}_2}} \mathbf{v}_{\text{oc},i} & \text{if } E + 1 \leq i \leq E + L, \end{cases} \\ R_{\text{sc},i} &= R_{a,i}^{-1}, \quad J_{\text{sc},i} = 0, \\ B_{\text{sc},i} &= \frac{z\rho F}{M_{\text{H}_2}}, \quad D_{\text{sc},i} = n_{c,i} \frac{\delta_{m,i}}{\sigma_{m,i} A_i} \frac{z^2 \rho^2 F^2}{M_{\text{H}_2}^2}. \end{aligned} \quad (19)$$

Note that the product of the electrolyzer input and output is equal to the electrical power

$$y_{\text{sc},i} u_{\text{sc},i} = \frac{z\rho F}{M_{\text{H}_2}} \mathbf{v}_i \mathbf{q}_{\text{sc},i} = \mathbf{i}_i \mathbf{v}_i,$$

for $i = 1, \dots, E$, whereas the output of the fuel cell model is $y_{\text{sc},i} = -\frac{z\rho F}{M_{\text{H}_2}} \mathbf{v}_i$ for all $i = E + 1, \dots, E + L$ reflecting the inverse relationship.

IV. PORT-HAMILTONIAN MODELING OF INTEGRATED HYDROGEN SYSTEMS

In this section, we interconnect the pH component models from Section III to obtain a pH model of the overall hydrogen grid. An example of such a grid is shown in Fig. 1.

The interconnected hydrogen grid without the sector coupling components is given by a combination of the pH models for the volumetric flow rate dynamics for \mathbf{q} that are given by (5), (12), (13) and the pH models for the pressure dynamics for \mathbf{p} that is given by (7), (8), (11).

Thus, we define the state vector assigned to nodes and representing (weighted) pressures at storage units, junctions and compressors as

$$x_n = ((x_{n,i})_{i=1}^S, (x_{n,i})_{i=S+1}^{S+F}, (x_{n,i})_{i=S+F+1}^N).$$

Likewise, the state vector collecting the volumetric flow rates at the different pipes and compressors is defined as

$$x_e = ((x_{e,i})_{i=1}^{M-2C}, (x_{e,i})_{i=M-2C+1}^M),$$

where without loss of generality we group the edges $e_f \in \mathcal{E}$ and $e_m \in \mathcal{E}$ corresponding to any compressor $n_i \in \mathcal{N}_C$, such that $m = f + 1$. Then, the overall system state vector is given by $x_g = (x_n, x_e)$.

The pressure dynamics of all components of the hydrogen grid can be written as a diagonal combination of all subsystems (7), (8) and (11), i.e.,

$$\dot{x}_n = (J_n - R_n) \nabla H_n(x_n) + B_n u_n, \quad (20)$$

$$y_n = B_n^\top \nabla H_n(x_n) = \begin{bmatrix} y_n^1 \\ y_n^2 \end{bmatrix} = \begin{bmatrix} \mathbf{p} \\ (\mathbf{p}_i)_{i=1}^{S+F} \end{bmatrix},$$

$$J_n = \text{diag}(J_{n,i})_{i=1}^N = 0_{N \times N}, \quad R_n = \text{diag}(R_{n,i})_{i=1}^N,$$

$$B_n = [B_n^1 \quad B_n^2] = \begin{bmatrix} I_N & 0_{C \times (S+F)} \\ 0_{C \times (S+F)} & I_{S+F} \end{bmatrix},$$

$$u_n = (u_n^1, \mathbf{q}_{\text{ex}}) := ((u_{n,i}^1)_{i=1}^N, (\mathbf{q}_{\text{ex},i})_{i=1}^{S+F}).$$

Furthermore, we rearrange the entries of the input vector such that u_n^1 collects all first entries of $u_{n,i}$ for all $i = 1, \dots, N$, which are precisely the volumetric flow differences and the Hamiltonian is given by $H_n = \sum_{i=1}^N H_{n,i}$.

Likewise, the volumetric flow rate dynamics of all components of the hydrogen grid can be written as a diagonal combination of all subsystems (5), (13) and (12), i.e.,

$$\dot{x}_e = (J_e - R_e(x_e)) \nabla H_e(x_e) + B_e u_e + d_e, \quad (21)$$

$$y_e = B_e^\top \nabla H_e(x_e) = \begin{bmatrix} y_e^1 \\ y_e^2 \end{bmatrix} = \begin{bmatrix} \mathbf{q} \\ (\mathbf{q}_{M+2(i-C)-1})_{i=1}^C \end{bmatrix},$$

$$J_e = \text{diag}(J_{e,i})_{i=1}^M = 0_{M \times M}, \quad R_e(x_e) = \text{diag}(R_{e,i}(x_{e,i}))_{i=1}^M,$$

$$B_e = [B_e^1 \quad B_e^2] = \begin{bmatrix} I_M & 0_{(M-2C) \times C} \\ \text{diag}([1 \quad 0]^\top)_{i=1}^C & I_C \end{bmatrix},$$

$$u_e = (u_e^1, \Delta \mathbf{p}) := ((u_{e,i}^1)_{i=1}^M, (\Delta \mathbf{p}_i)_{i=1}^C),$$

and the Hamiltonian is given by $H_e = \sum_{i=1}^M H_{e,i}$.

The interconnection of the node dynamics (20) and edge dynamics (21) is established via

$$u_n^1 = B_g \mathbf{q} = B_g y_e^1, \quad u_e^1 = -B_g^\top \mathbf{p} = -B_g^\top y_n^1,$$

which leads to the following pH model for the interconnected

hydrogen grid

$$\begin{aligned} \dot{x}_g &= (J_g - R_g(x_g))\nabla H_g(x_g) + B_g u_g + d_g, \\ y_g &= B_g^\top \nabla H_g(x_g) = \begin{bmatrix} (\mathbf{p}_i)_{i=1}^{S+F} \\ (\mathbf{q}_{M+2(i-C)-1})_{i=1}^C \end{bmatrix}, \quad u_g = \begin{bmatrix} \mathbf{q}_{\text{ex}} \\ \Delta \mathbf{p} \end{bmatrix}, \\ H_g(x_g) &= \sum_{i=1}^N H_{n,i}(x_n) + \sum_{i=1}^M H_{e,i}(x_e), \quad \nabla H_g(x_g) = \begin{bmatrix} \mathbf{p} \\ \mathbf{q} \end{bmatrix}, \\ R_g(x_g) &= \begin{bmatrix} R_n & 0_{N \times M} \\ 0_{M \times N} & R_e(x_e) \end{bmatrix}, \quad J_g = \begin{bmatrix} 0_{N \times N} & B_g \\ -B_g^\top & 0_{M \times M} \end{bmatrix}, \\ B_g &= \begin{bmatrix} B_n^2 & 0_{N \times C} \\ 0_{M \times (S+F)} & B_e^2 \end{bmatrix}, \quad d_g = \begin{bmatrix} 0_N \\ (d_{e,j})_{j=1}^M \end{bmatrix}. \end{aligned} \quad (22)$$

In the following, we add $E \geq 0$ electrolyzers which are connected to the storage units at $n_1, \dots, n_E \in \mathcal{N}_S$ and $L \geq 0$ fuel cells connected to the storage units at $n_{E+1}, \dots, n_{E+L} \in \mathcal{N}_S$ by setting $\mathbf{q}_{\text{sc}} = (\mathbf{q}_{\text{sc},i})_{i=1}^{E+L} = (\mathbf{q}_{\text{ex},i})_{i=1}^{E+L}$. For the resulting system, we keep the hydrogen volumetric flow rates \mathbf{q}_{sc} as input variables. This leads to the following sector-coupled hydrogen system with state vector $x_{cg} = (x_g, (x_{\text{sc},i})_{i=1}^{E+L})$

$$\begin{aligned} \dot{x}_{cg} &= (J_{cg} - R_{cg}(x_{cg}))\nabla H_{cg}(x_{cg}) + B_{cg} u_{cg} + d_{cg,1}, \\ y_{cg} &= B_{cg}^\top \nabla H_{cg}(x_{cg}) + D_{cg} u_{cg} + d_{cg,2}, \\ R_{cg}(x_{cg}) &= \begin{bmatrix} R_g(x_g) & 0_{(N+M) \times (E+L)} \\ 0_{(E+L) \times (N+M)} & R_{\text{sc}} \end{bmatrix}, \\ J_{cg} &= \begin{bmatrix} J_g & 0_{(N+M) \times (E+L)} \\ 0_{(E+L) \times (N+M)} & 0_{(E+L) \times (E+L)} \end{bmatrix}, \\ u_{cg} &= \begin{bmatrix} \mathbf{q}_{\text{sc}} \\ (\mathbf{q}_{\text{ex},i})_{i=E+L+1}^{S+F} \\ (\Delta \mathbf{p}_i)_{i=1}^C \end{bmatrix}, \\ B_{cg} &= \begin{bmatrix} B_g \\ \begin{bmatrix} \frac{z\rho F}{M_{\text{H}_2}} I_{E+L} & 0_{(E+L) \times (N-E-L)} \end{bmatrix} \end{bmatrix}, \\ d_{cg,1} &= (d_g, 0_{E+L}), \quad d_{cg,2} = ((d_{\text{sc},i})_{i=1}^{E+L}, 0_{N-E-L}), \\ D_{cg} &= \begin{bmatrix} \text{diag}(D_{\text{sc},i})_{i=1}^{E+L} & 0_{(E+L) \times (N-E-L)} \\ 0_{(N-E-L) \times (E+L)} & 0_{(N-E-L) \times (N-E-L)} \end{bmatrix}, \end{aligned} \quad (23)$$

and with the overall Hamiltonian

$$H_{cg}(x_{cg}) = H_g(x_g) + \sum_{i=1}^{E+L} H_{\text{sc},i}(x_{\text{sc},i}).$$

V. CONCLUSION

In this work, we have presented a unified systematic port-Hamiltonian (pH) framework for modeling hydrogen systems, including storage units, electrolyzers, fuel cells, compressors, and pipelines. The inherent passivity properties of pH systems open the door to a structured analysis and controller synthesis for this emerging class of new energy systems. In future work, we will focus on further refining the presented modeling approach, especially by relaxing some of the assumptions made and complementing the hydrogen system with an explicit pH representation of the electrical power system.

REFERENCES

- [1] F. Neumann, E. Zeyen, M. Victoria, and T. Brown, "The potential role of a hydrogen network in Europe," *Joule*, vol. 7, no. 8, pp. 1793–1817, 2023.
- [2] M. Yue, H. Lambert, E. Pahon, R. Roche, S. Jemei, and D. Hissel, "Hydrogen energy systems: A critical review of technologies, applications, trends and challenges," *Renewable and Sustainable Energy Reviews*, vol. 146, p. 111180, 2021.
- [3] Vereinigung der Fernleitungsnetzbetreiber Gas e.V., "Joint application for the hydrogen core network," July 2024.
- [4] F. Dawood, M. Anda, and G. Shafuallah, "Hydrogen production for energy: An overview," *International Journal of Hydrogen Energy*, vol. 45, no. 7, pp. 3847–3869, 2020.
- [5] A. Schaft and D. Jeltsema, "Port-Hamiltonian systems theory: An introductory overview," *Found. Trends Syst. Control*, 2014.
- [6] S. Fiaz, D. Zonetti, R. Ortega, J. M. A. Scherpen, and A. J. van der Schaft, "A port-Hamiltonian approach to power network modeling and analysis," *Eur. J. Control*, vol. 19, no. 6, pp. 477–485, 2013.
- [7] J. Schiffer, R. Ortega, A. Astolfi, J. Raisch, and T. Sezi, "Conditions for stability of droop-controlled inverter-based microgrids," *Automatica*, vol. 50, no. 10, pp. 2457–2469, 2014.
- [8] H. Gernandt, B. Severino, X. Zhang, V. Mehrmann, and K. Strunz, "Port-Hamiltonian modeling and control of electric vehicle charging stations," *IEEE Transactions on Transportation Electrification*, vol. 11, no. 1, pp. 2897–2907, 2025.
- [9] S.-A. Hauschild, N. Marheineke, V. Mehrmann, J. Mohring, A. M. Badlyan, M. Rein, and M. Schmidt, "Port-Hamiltonian modeling of district heating networks," in *Progress in differential-algebraic equations II*, pp. 333–355, Springer, 2020.
- [10] F. Strehle, J. E. Machado, M. Cucuzzella, A. J. Malan, J. M. Scherpen, and S. Hohmann, "Port-Hamiltonian modeling of hydraulics in 4th generation district heating networks," in *2022 IEEE 61st Conference on Decision and Control (CDC)*, pp. 1182–1189, IEEE, 2022.
- [11] A. Krishna and J. Schiffer, "A port-Hamiltonian approach to modeling and control of an electro-thermal microgrid," *IFAC-PapersOnLine*, vol. 54, no. 19, pp. 287–293, 2021.
- [12] P. Domschke, J. Giesselmann, J. Lang, T. Breiten, V. Mehrmann, R. Morandin, B. Hiller, and C. Tischendorf, "Gas network modeling: An overview (extended english version)," February 2023. Preprint.
- [13] A. J. Malan, L. Rausche, F. Strehle, and S. Hohmann, "Port-Hamiltonian modelling for analysis and control of gas networks," *IFAC-PapersOnLine*, vol. 56, no. 2, pp. 5431–5437, 2023.
- [14] A. J. Malan, A. Gießler, F. Strehle, and S. Hohmann, "Passivity-based pressure control for grid-forming compressors in gas networks," in *2024 European Control Conference (ECC)*, pp. 1097–1104, 2024.
- [15] T. Bendokat, P. Benner, S. Grundel, and A. S. Nayak, "Modelling gas networks with compressors: A port-Hamiltonian approach," *PAMM*, vol. 24, no. 4, p. e202400164, 2024.
- [16] L. Kumar, J. Chen, C. Wu, Y. Chen, and A. van der Schaft, "A segmented model based fuel delivery control of PEM fuel cells: A port-Hamiltonian approach," *Automatica*, vol. 168, p. 111814, 2024.
- [17] D. Sbarbaro, "On the port-Hamiltonian models of some electrochemical processes," *IFAC-PapersOnLine*, vol. 51, no. 3, pp. 38–43, 2018.
- [18] A. van der Schaft, *L₂-Gain and Passivity Techniques in Nonlinear Control*. Springer, 2017.
- [19] K. Pambour, R. Bolado-Lavin, and G. Dijkema, "An integrated transient model for simulating the operation of natural gas transport systems," *Journal of Natural Gas Science and Engineering*, vol. 28, pp. 672–690, 2016.
- [20] N. Klopčič, K. Esser, J. F. Rauh, M. Sartory, and A. Trattner, "Modelling hydrogen storage and filling systems: A dynamic and customizable toolkit," *International Journal of Hydrogen Energy*, vol. 49, pp. 1180–1195, 2024.
- [21] J. T. Gravdahl and O. Egeland, "Passivity based compressor surge control using a close-coupled valve," *Proceedings of the 1997 COSY Workshop on Control of Nonlinear and Uncertain Systems*. Zurich, Switzerland, pp. 139–143, 1997.
- [22] M. Espinosa-López, C. Darras, P. Poggi, R. Glises, P. Baucour, A. Rakotondrainibe, S. Besse, and P. Serre-Combe, "Modelling and experimental validation of a 46 kW PEM high pressure water electrolyzer," *Renewable Energy*, vol. 119, pp. 160–173, 2018.
- [23] G. Lichtenberg, G. Pangalos, C. C. Yáñez, A. Luxa, N. Jöres, L. Schnelle, and C. Kaufmann, "Implicit multilinear modeling: An introduction with application to energy systems," *at - Automatisierungstechnik*, vol. 70, no. 1, pp. 13–30, 2022.
- [24] M. Espinosa-López, C. Darras, P. Poggi, R. Glises, P. Baucour, A. Rakotondrainibe, S. Besse, and P. Serre-Combe, "Modelling and experimental validation of a 46 kW PEM high pressure water electrolyzer," *Renewable Energy*, vol. 119, pp. 160–173, 2018.

- [25] J. Pukrushpan, H. Peng, and A. Stefanopoulou, "Simulation and analysis of transient fuel cell system performance based on a dynamic reactant flow model," ASME Int. Mech. Eng. Congress Expo., vol. 2, 01 2002.
- [26] M. Carmo and D. Stolten, "Chapter 4 - energy storage using hydrogen produced from excess renewable electricity: Power to hydrogen," in Science and Engineering of Hydrogen-Based Energy Technologies (P. E. V. de Miranda, ed.), pp. 165–199, Academic Press, 2019.
- [27] M. Pfennig, B. Schiffer, and T. Clees, "Thermodynamical and electrochemical model of a PEM electrolyzer plant in the megawatt range with a literature analysis of the fitting parameters," International Journal of Hydrogen Energy, vol. 104, pp. 567–583, 2025.
- [28] H. Ramirez and Y. Le Gorrec, "An overview on irreversible port-Hamiltonian systems," Entropy, vol. 24, no. 10, 2022.
- [29] B. Yodwong, D. Guilbert, M. Hinaje, M. Phattanasak, W. Kaewmanee, and G. Vitale, "Proton exchange membrane electrolyzer emulator for power electronics testing applications," Processes, vol. 9, no. 3, 2021.